Spatial Structure and Formation Mechanism of Local Winds "Suzuka-oroshi" at the Foothills of Suzuka Mountains, Japan

Shunsuke YAMADA

Graduate School of Life and Environmental Sciences, University of Tsukuba, Tsukuba, Japan

and

Hiroyuki KUSAKA

Center for Computational Sciences, University of Tsukuba, Tsukuba, Japan

(Manuscript received 22 June 2021, in final form 21 May 2022)

Abstract

We examined the essential features and formation mechanism of the strong local "Suzuka-oroshi" winds, which are located leeward of the Suzuka Mountains in Japan. This area features favorable topography for downslope windstorms. Climatological analysis revealed that Suzuka-oroshi mainly occurred after an extratropical cyclone with a cold front and passed the Sea of Japan (55 % of all occurrences). Additionally, inversion layers (1–5 km level) were observed in 74 % of cases. Climatological analysis using spatially dense observational data revealed that the strongest winds tended to blow in the northern part of the plain on the leeward side. Numerical simulations for one case by the Weather Research and Forecasting (WRF) model with a 1 km grid increment supported this finding. Simulation results with and without the Suzuka Mountains demonstrated that the strong Suzuka-oroshi in the northern part of the plain comprised downslope windstorms with a transition of flow regime (the internal Froude number was lesser than 1.0 at the windward of mountains and greater than 1.0 above the leeward slope). Additionally, the differences in the height of the mountains between the northern and southern parts resulted in greater wind speed in the northern parts compared to the southern parts.

Keywords Suzuka-oroshi; local wind; downslope windstorm; local hydraulic theory; mountain wave

Citation Yamada, S., and H. Kusaka, 2022: Spatial structure and formation mechanism of the local winds "Suzuka-oroshi" at the foothills of the Suzuka Mountains, Japan. *J. Meteor. Soc. Japan*, **100**, 751–766, doi:10.2151/jmsj.2022-039.

1. Introduction

Downslope windstorms are strong local winds that blow on the leeward slopes and foothills of mountains and are formed by the acceleration of air as they cross the mountains. These winds occur in many places worldwide, including Foehn in the Alps (Gohm and Mayr 2004; Zängl et al. 2004; Armi and Mayr 2007), Bora on the Adriatic coast (Yoshino 1975; Smith 1985, 1987; Gohm and Mayr 2005), Chinook in the Rocky Mountains (Glenn 1961; Lilly and Zipser 1972), and Antarctic Peninsula foehns (Orr et al. 2008; Elvidge et al. 2016, 2020; Turton et al. 2018).

Theories for explaining the occurrence of downslope windstorms were proposed in the 1980s, and they can be broadly summarized into two or three main theories (Durran 1990; Jackson et al. 2013; Lin

Corresponding author: Hiroyuki Kusaka, Center for Computational Sciences, University of Tsukuba, 1-1-1 Tennoudai, Tsukuba, Ibaraki 305-0006, Japan
E-mail: kusaka@ccs.tsukuba.ac.jp
J-stage Advance Published Date: 21 June 2022

2007). First is the local hydraulic theory (e.g., Smith 1985; Durran 1986) that extends classical shallow water theory (Houghton and Kasahara 1968; Arakawa 1968, 1969) to the atmosphere with stratification. In this theory, the flow in the lower layers of the well-mixed region, such as the wave-breaking region, behaves locally as a shooting (supercritical) flow. Specifically, flows approaching the mountains are divided by the well-mixed region above the mountains and accelerate below this region. Second is the resonant amplification theory that was proposed in a series of studies conducted by Peltier and Clark (Peltier and Clark 1979, 1983; Clark and Peltier 1984). They reported that the severe downslope windstorms occur because of nonlinear resonance between the upward and downward mountain waves reflected at the critical layer. The third is the vertical energy transport theory that is linear theory (Klemp and Lilly 1975). Durran and Klemp (1987) examined the critical level height for a stage of a severe downslope windstorm state, whose results supported Smith's theory. Currently, it is considered that Peltier–Clark's and Smith's theories explain flows at the earlier and mature stages of severe downslope windstorm development, respectively (Lin 2007).

Downslope windstorms easily occur in straight mountain ranges and in terrains where the leeward slope is steeper than the windward slope (Raymond 1972; Lilly and Klemp 1979; Pitts and Lyons 1989; Miller and Durran 1991; Saito and Ikawa 1991). Furthermore, downslope windstorms easily occur over mountains with saddles because hydraulic jumps are less likely to occur leeward of saddles and strong wind regions extend farther leeward (Raymond 1972; Lilly and Klemp 1979; Pitts and Lyons 1989; Miller and Durran 1991; Saito 1993; Gohm et al. 2008; Elvidge and Renfew 2016).

The conditions favored by downslope windstorms are affected by the terrain shape and atmospheric condition. The mountain Froude number Fr (or its inverse, the nondimensional mountain height) is often used as an indicator of the occurrence of downslope windstorms and/or mountain-wave breaking. Lin and Wang (1996) investigated the relationship between Fr and the behavior of airflows over mountains using a two-dimensional idealized model (Eq. 1).

$$Fr = U/NH. \tag{1}$$

Here, U is the wind speed of the approaching flow, N is the Brunt–Väisälä frequency, and H is the mountain height. Lin and Wang (1996) found that downslope windstorms occur when Fr is approximately 0.6–1.2, and other studies showed similar results (Gabersek and Durran 2004). The presence of a temperature inversion layer and critical layer facilitates the formation of downslope windstorms (Klemp and Durran 1987; Smith and Skyllingstad 2011). The role of the inversion layer in downslope windstorm occurrences can be approximately divided into the following two categories. In the presence of an inversion layer at a lower level, the airflow over the mountains easily transitions from subcritical flow to supercritical flow, facilitating the occurrence of downslope windstorms. The presence of an inversion layer at the upper level also facilitates mountain-wave breaking just below this layer because of the reflection and resonance of mountain waves, thereby making it easier for downslope windstorms to blow under the well-mixed region.

Downslope windstorms are common in Japan because of the complex and undulating topographies of the country's islands, which are unique to each region. Japan's well-known downslope windstorms include the "Yamaji-kaze" (Saito and Ikawa 1991; Saito 1993, 1994), "Hiroto-kaze" (Fudeyasu et al. 2008), "Karakkaze" (Yoshino 1975, 1986; Kusaka et al. 2011; Nishi and Kusaka 2019a, b), "Inami-kaze" (Koyanagi and Kusaka 2020), "Jintsu-oroshi" (Kusaka et al. 2021), "Zao-oroshi" (Sawada et al. 2012), "Chokai-oroshi" (Asano and Kusaka 2022), and "Suzuka-oroshi" (Owada 1990; Komatsu and Tachibana 2016). The "Kiyokawa-dashi" seems to be the gap wind but exhibits characteristics of downslope windstorms (Yoshino 1986; Ishii et al. 2007; Sasaki et al. 2005, 2010). Japan's local winds, including downslope windstorms, have been summarized by Yoshino (1986) and Kusaka and Fudeyasu (2017).

A strong westerly wind, "Suzuka-oroshi", blows in the eastern plains at the base of the Suzuka Mountains (Yoshino 1975). The Suzuka Mountains are in the Mie and Shiga prefectures and are north–south oriented (Fig. 1). These mountains are divided into three parts: the northern part comprises a series of mountains that are ~ 1,000 m in height, mountains in the central part are ~ 500 m in height, and those in the southern part are ~ 800 m in height. The Suzuka Pass, a major transportation hub with highways, is in the central part of the Suzuka Mountains. The Suzuka Mountains are a highly asymmetric range; the eastern slopes are steeper than the western slopes. Therefore, the terrain of the Suzuka Mountains can make them prone to downslope windstorms.

Owada (1990) clarified the climatological characteristics of Suzuka-oroshi using Automated Meteo-

rological Data Acquisition System (AMeDAS) data for the area to the south (i.e., leeward) of the Suzuka Mountains. He identified Suzuka-oroshi as winds with surface wind speeds of at least 8 m s^{-1} and found that Suzuka-oroshi was more likely to blow during winter and spring in the daytime under a typical pressure pattern in winter (that is a pressure pattern with the Siberian High to the west of Japan, a low to the east of Japan) (Figs. 2a, b). The analysis of the distribution of the wind-shaped trees (wind-deformed tree) showed that Suzuka-oroshi tends to blow in the central and southern parts of the plain that is located at the leeward of the Suzuka Mountains. Komatsu and Tachibana (2016) also reported that Suzuka-oroshi blows in the southern part of the plain using the AMeDAS surface wind data. Although Suzuka-oroshi has been studied, four open questions remain at least.

The first question concerns the spatial distribution of Suzuka-oroshi. According to the principal of the local elementary school and the fire department officer living in the areas shown in Fig. 1, Suzuka-oroshi blows in the leeward area of the northern part of the Suzuka Mountains. These local residents' perceptions are inconsistent with the results of the previous studies (Owada 1990; Komatsu and Tachibana 2016).

The second question concerns the favorable synoptic weather pattern during Suzuka-oroshi events. Owada (1990) analyzed the synoptic weather pattern when the surface wind speed was 8 m s^{-1} or higher (Figs. 2a, b). However, according to our interviews, the local people recognize Suzuka-oroshi as strong enough to cause large branches of trees to sway, power lines to roar, and people to feel threatened. This is equivalent to a wind speed of 11 m s^{-1} on the Beaufort Scale: "The large branches of the trees sway, making it difficult to hold an umbrella. Power lines squeal" (strong breeze, wind speed 10.8–13.8 m s^{-1} at 10 m above ground). Therefore, Owada (1990) might not have captured the typical pressure pattern that occurs when Suzuka-oroshi blows.

The third and fourth questions are regarding the favorable mesoscale atmospheric conditions for Suzuka-oroshi and their formation mechanisms. The relationship between Suzuka-oroshi, the inversion layer, and *Fr* remains unclear. Regarding the mechanism of Suzuka-oroshi, Komatsu and Tachibana (2016) launched six sondes simultaneously, used AMeDAS surface wind data, and made a hypothesis that Suzuka-oroshi was a downslope windstorm with hydraulic jumps and gap winds. They observed the downslope winds but were unable to observe the gap winds. Therefore, it remains unclear whether Suzuka-oroshi is a downslope windstorm or a gap wind.

On the basis of the previous studies, this study was conducted to determine where the Suzuka-oroshi winds blow strongly, the favorable atmospheric conditions for the formation of Suzuka-oroshi, and the major formation mechanism of Suzuka-oroshi (either downslope windstorms or gap winds).

2. Data and method

2.1 Climatological analysis

We identified Suzuka-oroshi as the wind direction of south–southwest to north–northwest and a wind speed of 11 m s^{-1} or higher on the east side of the Suzuka Mountains, defined as the time when the wind was blowing on the leeward side of the Suzuka Mountains. Additionally, we considered any continuous period during which Suzuka-oroshi was blowing as a Suzuka-oroshi case. When the interruption time was less than 3 h, the interruption time was ignored, and the data collected before and after the interruption were combined into one case. The lower limit of the wind speed for Suzuka-oroshi was set to match the reported feelings of local residents as local winds are recognized and named by the people living in the area. Therefore, we first interviewed the local residents, who revealed that the strong wind causing the power lines to roar and inducing fear in people is named Suzuka-oroshi. This feeling is expressed using the Beaufort Scale: strong breeze, wind speed 10.8–13.8 m s^{-1} at 10 m above ground. Therefore, we set 11 m s^{-1} as the lower limit of the wind speed of Suzuka-oroshi. Additionally, to compare our results with those of previous studies, Weak-Suzuka-oroshi was extracted under a wind speed of 8 m s^{-1} and analyzed using the same approach as used for Suzuka-oroshi with more than 11 m s^{-1} wind speed.

However, because the installation heights of the anemometers differed at each observation point, the wind speed observed at each location was converted to the wind speed at 10 m above ground level using the following power-law formula (Eq. 2):

$$U_{10} = U_z (10/Z)^{\alpha}. \tag{2}$$

Here, U_{10} is the wind speed at 10 m above ground, U_z is the observed wind speed, Z is the observed height, and α is a parameter representing the surface roughness and atmospheric stability in the surface layer. α was set to 0.25, which is used for winds over forests, urban areas without tall buildings, and residential areas (Wind Engineering Institute1984). Unless otherwise noted, the surface wind speed was defined as the wind speed at 10 m above ground

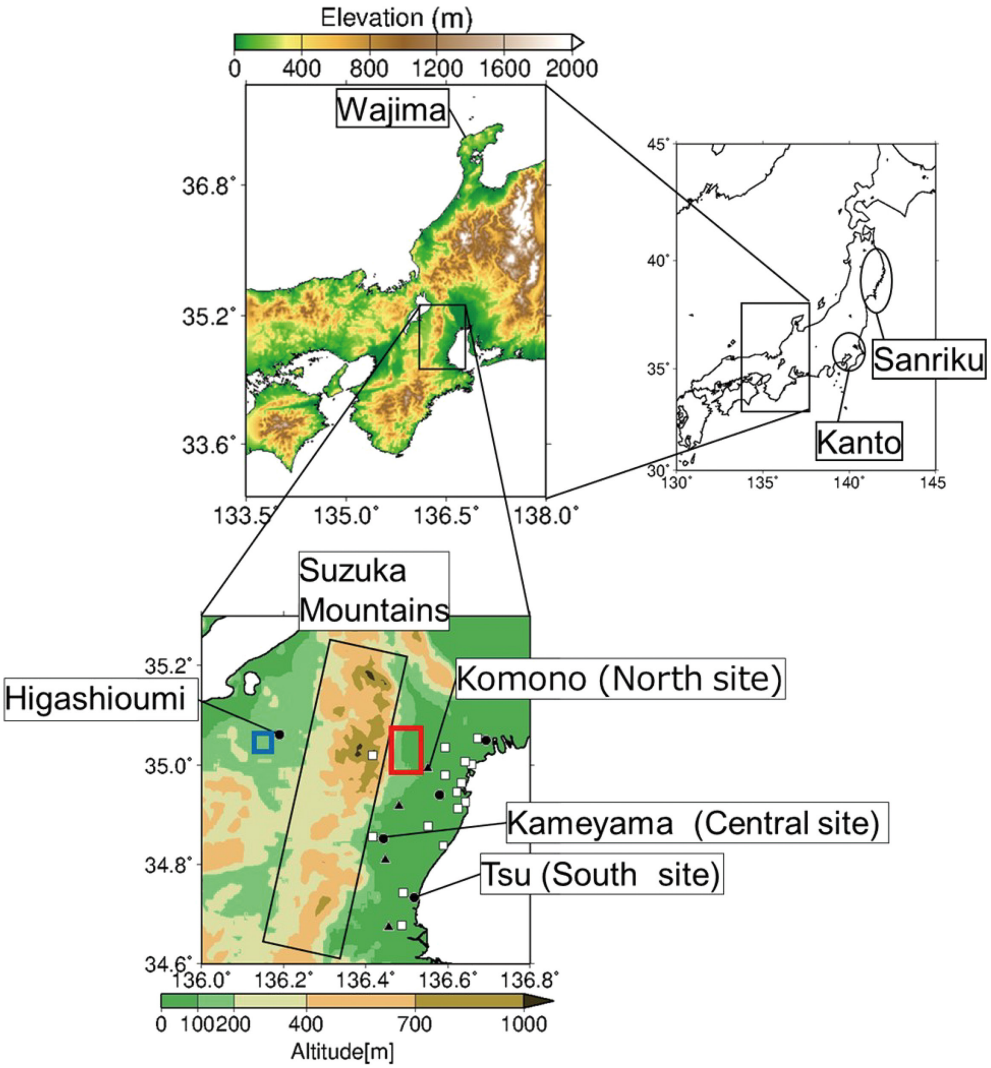

Fig. 1. Topography around the Suzuka Mountains and observation points for the data used.

Table 1. Surface observation data.

	Number of points	Period	Time interval
● AMeDAS	5		
□ Atmospheric Environmental Regional Observation System	15	2012/1/1–2016/12/31	10 min
▲ Observation point on the highways	4		

level. The surface observation data are summarized in Fig. 1 and Table 1. Along with the data from the Japan Meteorological Agency's AMeDAS, we used the Ministry of the Environment's data (Atmospheric Environmental Regional Observation System) and the data observed at highways. The data period was from January 1, 2012 to December 31, 2016 with data intervals of 10 min for AMeDAS and Atmospheric Environmental Regional Observation System and 5 min for highways.

We first investigated the spatial distribution of Suzuka-oroshi and then surveyed a typical weather pattern when Suzuka-oroshi was blowing. The seasonal and time-dependent characteristics of Suzuka-

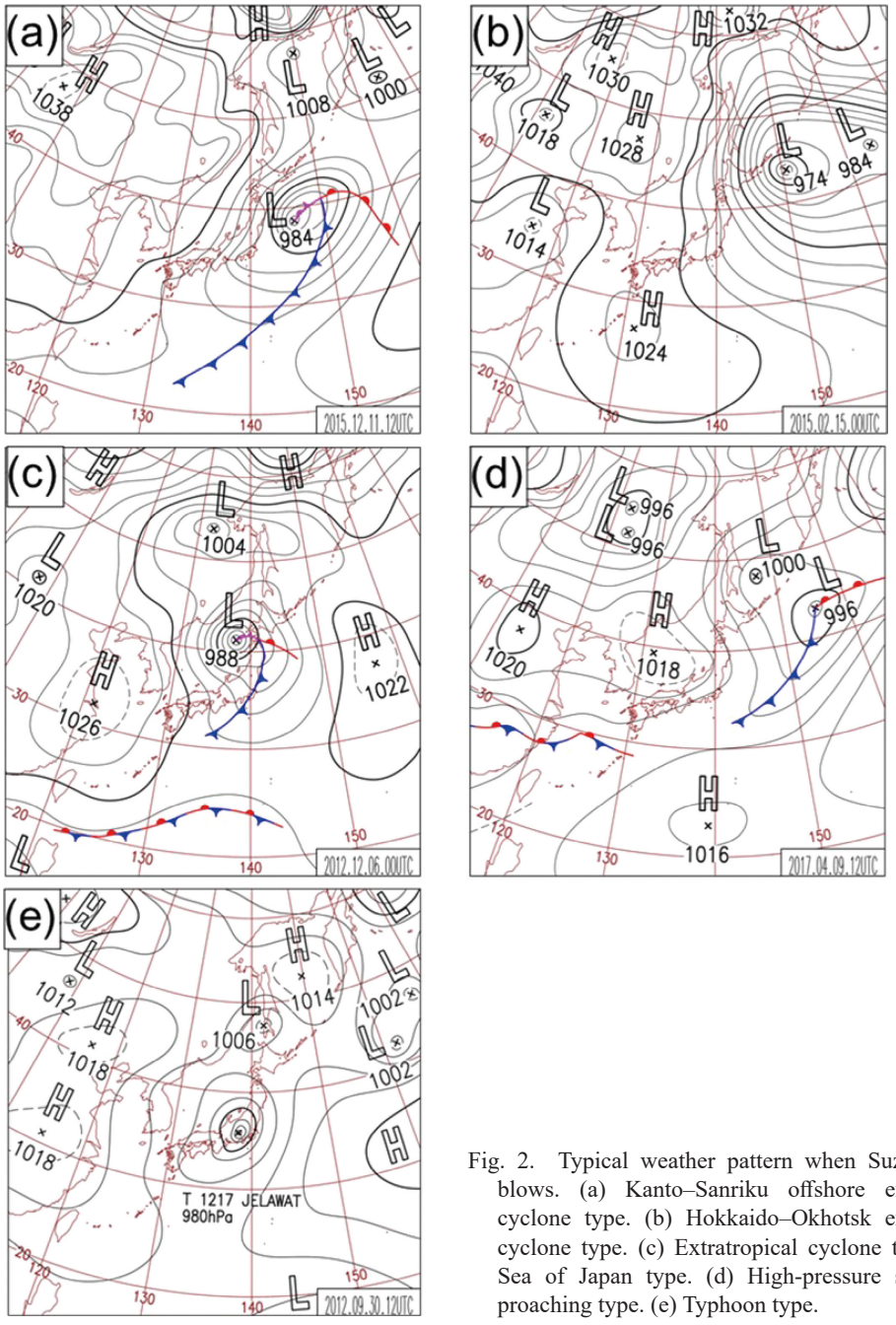

Fig. 2. Typical weather pattern when Suzuka-oroshi blows. (a) Kanto–Sanriku offshore extratropical cyclone type. (b) Hokkaido–Okhotsk extratropical cyclone type. (c) Extratropical cyclone through the Sea of Japan type. (d) High-pressure system approaching type. (e) Typhoon type.

oroshi were also investigated. Third, we examined the location wherein Suzuka-oroshi occurred. Finally, we investigated the presence or absence of an inversion layer using radiosonde observation data at Wajima, whose location is shown in Fig. 1. At Wajima observatory, sonde observations are performed at 0900 and 2100 Japan Standard Time (JST). We defined an inversion layer as any layer wherein the temperature increases as the altitude increases at 1–5 km level in the sonde data. The wind speed approaching the mountains was calculated using the westerly wind component at the 950 hPa level over the windward mountains shown in Fig. 1 as a blue square just before or just after the onset of Suzuka-oroshi. As the wind component, we used mesoscale analysis data with horizontal resolutions of 5 km and time resolutions of

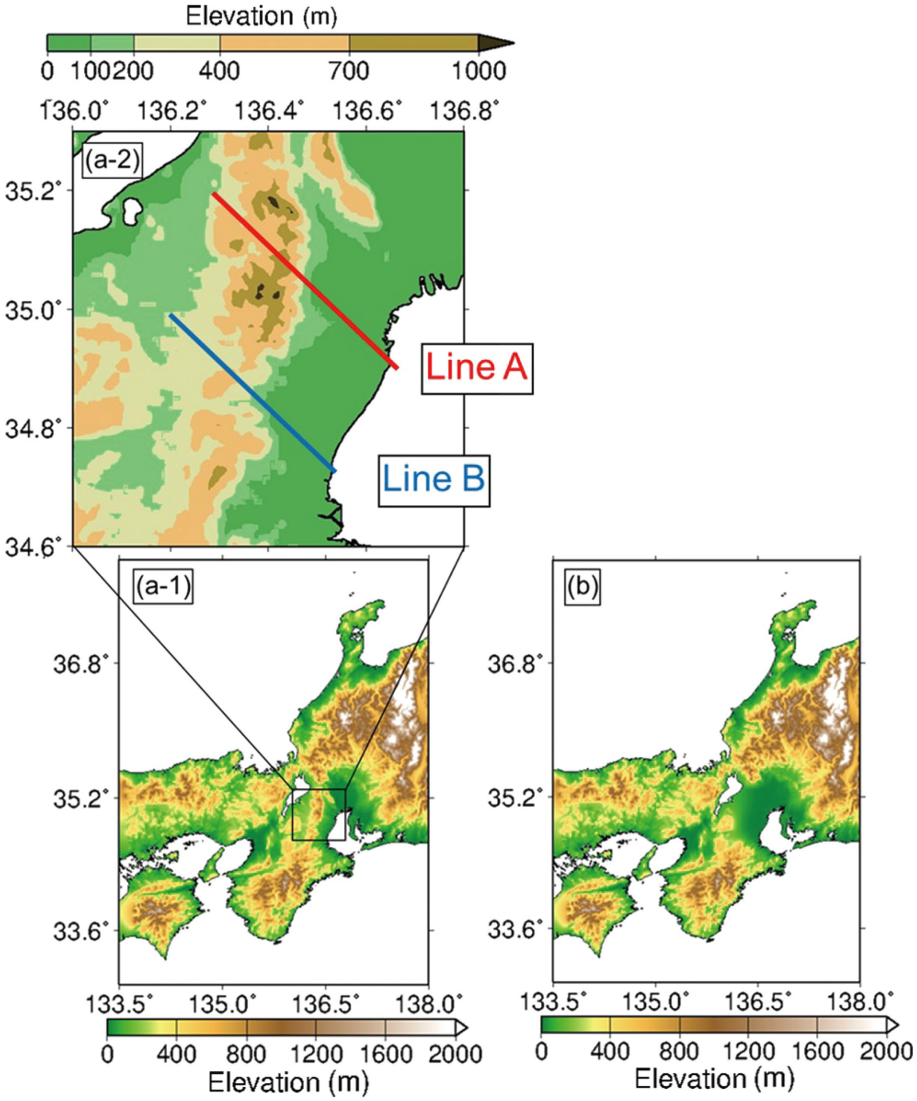

Fig. 3. Topography used in the numerical simulations. (a) Control experiment (Case CTRL). (b) Experiment without Suzuka Mountains (Case NoMt).

3 h, provided by Japan Meteorological Agency (JMA).

2.2 Numerical simulations

To further investigate the effects of the Suzuka Mountains on Suzuka-oroshi events, we conducted numerical simulations using the Weather Research and Forecasting (WRF) model and covered a case that occurred on March 5–6, 2014, which was named as the CTRL. We also simulated a case wherein the Suzuka Mountains were excluded from the topographic data, named as case NoMt. Figure 3 shows the simulation domain and topographic settings of the two simulation cases. The domain comprised 398 × 648 grid points with a horizontal grid spacing of 1.0 km. The domains had 50 vertical sigma levels, and the model top was 100 hPa. The initial and boundary conditions were obtained from mesoscale analysis data. The model configurations are summarized in Table 2.

3. Results

3.1 Climatological analysis

Figure 2 shows typical weather patterns when Suzuka-oroshi is blowing. Suzuka-oroshi tended to occur when an extratropical cyclone with a cold front

Table 2. Model configuration.

Model	WRF model, version 3.9.1
Grid spacing	1.0 km
Number of grid points	398 × 648 grid points
Number of vertical layers	50 vertical sigma levels
Boundary layer scheme	Yonsei University (YSU) PBL scheme
Simulation period (JST)	2014/03/05/ 0300–2014/03/07 0300
Initial/boundary condition	JMA-mesoscale analysis
Land use and terrain height	GSI digital national land information

Table 3. Breakdown of typical weather patterns during Suzuka-oroshi events.

	Number of Suzuka-oroshi events
"Kanto-Sanriku extratropical cyclone type" (Fig. 2a)	7
"Hokkaido-Okhotsk extratropical cyclone type" (Fig. 2b)	2
"Extratropical cyclone through Sea of Japan type" (Fig. 2c)	27
"High-pressure approaching type" (Fig. 2)	2
"Typhoon type" (Fig. 2e)	6
Other	1

passed over the Sea of Japan (Fig. 2c). This was the primary weather pattern in 27 cases (55 % of cases) (Table 3). The second typical weather pattern was an extratropical cyclone type but was located offshore of Kanto and Sanriku (Fig. 2a), which comprised seven cases (16 % of cases). Other types of weather patterns included the typhoon type (Fig. 2e). Conversely, the primary weather pattern of the Weak-Suzuka-oroshi is an extratropical cyclone located offshore of Kanto and Sanriku (Fig. 2a). This type accounts for 147 cases (36 % of cases).

Figure 4 shows the seasonal and time-dependent characteristics of Suzuka-oroshi. As shown in Fig. 4a, the frequency of Suzuka-oroshi was highest during spring (March to April) and lowest in summer (June to August), although the sample size may not be large enough. In Japan, extratropical cyclones and associated cold fronts often pass through these areas in spring. The frequency of Weak-Suzuka-oroshi supports this tendency in Owada (1990) (Fig. 4b). Suzuka-oroshi tended to occur in the late afternoon, but this time, dependency was weaker than that of Weak-Suzuka-oroshi (Figs. 4c, d).

We then examined the location where Suzuka-oroshi tended to blow. The results of the climatological survey (Figs. 5a, b) showed that in the northern part of the plain, Suzuka-oroshi blows most frequently around Komono, which is inland in the foothills of the Suzuka Mountains. It rarely blows near the northern part of the plain along the coast. In the southern and central parts, it blows anywhere. Additionally, the wind direction was mostly northwest at most locations during Suzuka-oroshi events. Conversely, Weak-Suzuka-oroshi occurs anywhere on the plain (Figs. 5c, d).

We also compared the wind speeds on the windward and leeward sides of the Suzuka Mountains during Suzuka-oroshi events; the results are shown in Fig. 6. The mean wind speed was ~ 5 m s^{-1} higher at Tsu on the leeward side of the mountains than at Higashiomi on the windward side. Thus, the wind speed may increase after passing over the mountains. Conversely, in the case of Weak-Suzuka-oroshi, the difference in wind speed between the windward and leeward mountains was small. These results suggest that the presence of the mountains is responsible for the strong winds of Suzuka-oroshi.

However, this does not reveal whether Suzuka-oroshi is a downslope wind. Therefore, we investigated whether the environmental field during the Suzuka-oroshi event was favorable for generating downslope windstorms.

Table 4 shows that an inversion layer at 1–5 km level was present in 31 Suzuka-oroshi cases (74 % of cases). This result agrees with the tendency of weather patterns in which Suzuka-oroshi often occurs when an extratropical cyclone with a cold front passes over the Sea of Japan. The wind speed approaching the mountains ranged from 6 m s^{-1} to 12 m s^{-1} in 23 cases (55 % of cases). Conversely, there were nine cases (21 % of cases) wherein there was no inversion layer at 1–5 km. We calculated *Fr* in these four cases using the

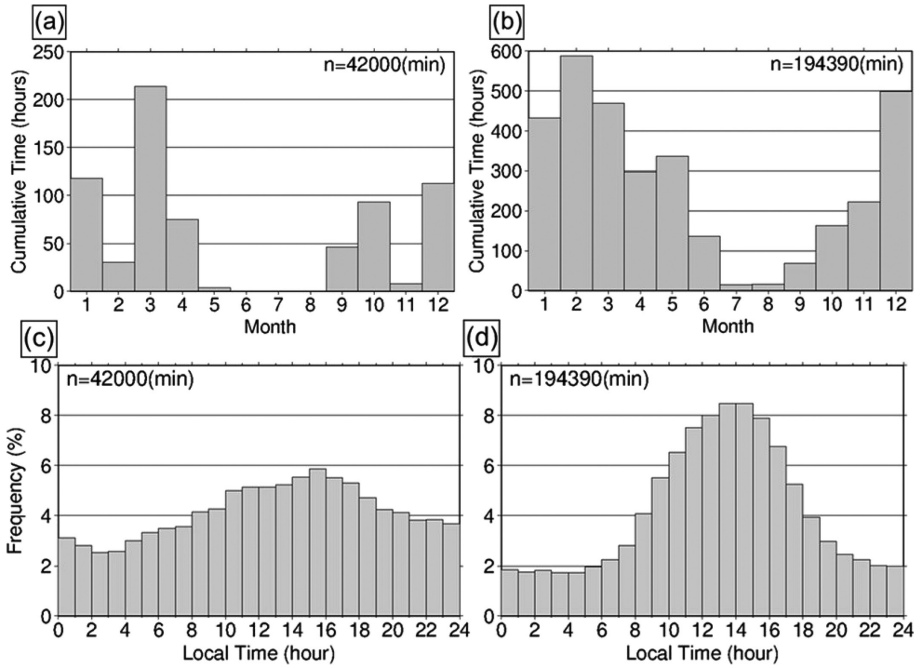

Fig. 4. Frequency of Suzuka-oroshi events by month and time from 2012 to 2016. (a) Monthly frequency of Suzuka-oroshi. (b) Monthly frequency of Weak-Suzuka-oroshi. (c) Hourly frequency of Suzuka-oroshi. (d) Hourly frequency of Weak-Suzuka-oroshi.

wind speed data, Brunt–Väisälä frequency N, and the mountain height H that was set to 1000 m. Fr values were 0.8–1.4, which are favorable for the downslope windstorms. Thus, most Suzuka-oroshi cases occurred under favorable atmospheric conditions for downslope windstorms.

3.2 Numerical simulations

The simulation case was a strong wind event on March 5, 2014, which is a typical case during a cyclone with a cold front passing over the Sea of Japan (Fig. 7). There was no inversion layer but a slightly strong stable layer around 1.5–2.0 km at the windward side during the events. The inflow wind speed was within 6–12 m s^{-1}.

First, we confirmed the reproducibility of the temporal variations in the wind direction and speed obtained from the CTRL simulation. We included the results of the comparison at Tsu and Komono, where strong winds were observed. Figure. 8 shows that the wind speed suddenly increased around 1600 JST on March 5, 2014, when the 10-min average wind speed exceeded 11 m s^{-1}. The time series of the observed wind direction shows that the wind direction varied before the strong winds blew; however, after the strong winds began blowing, the wind direction remained stable in the northwest. This time series variation is a characteristic of downslope windstorms. Comparison of the simulated results with the observations showed that the WRF model could reproduce the characteristics of the observed time series of surface winds.

Second, we examined the reproducibility of the spatial distribution of surface winds obtained from the CTRL simulation. The observations indicate that northwesterly strong winds blew in the southern and central parts of the plains and northern foothills area (Fig. 9a). There were weaker wind areas in the northern part of the plain near the coast than in the surroundings.

The numerical simulation results showed that the simulated wind speed was slightly higher than the observed speed (Fig. 9b). However, strong wind areas in the central and southern parts of the plains and the northern area near the foothills were well represented. The WRF model also reproduced the spatial characteristics of the winds observed when the strong winds began to blow. Comparison results at other times are shown in Appendix A.

After confirming that the WRF model reproduced

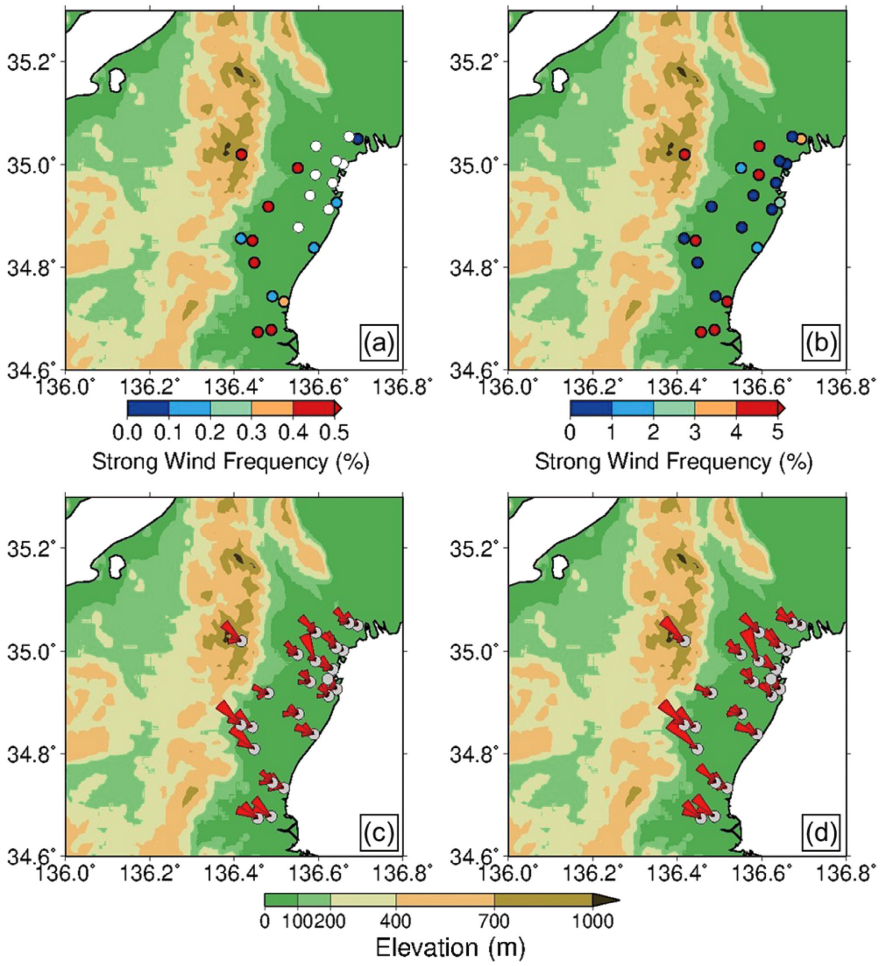

Fig. 5. Map of the frequency of Suzuka-oroshi events and wind rose at each location. (a) Frequency of Suzuka-oroshi. (b) Frequency of Weak-Suzuka-oroshi. (c) Wind rose of Suzuka-oroshi. (d) Wind rose of Weak-Suzuka-oroshi.

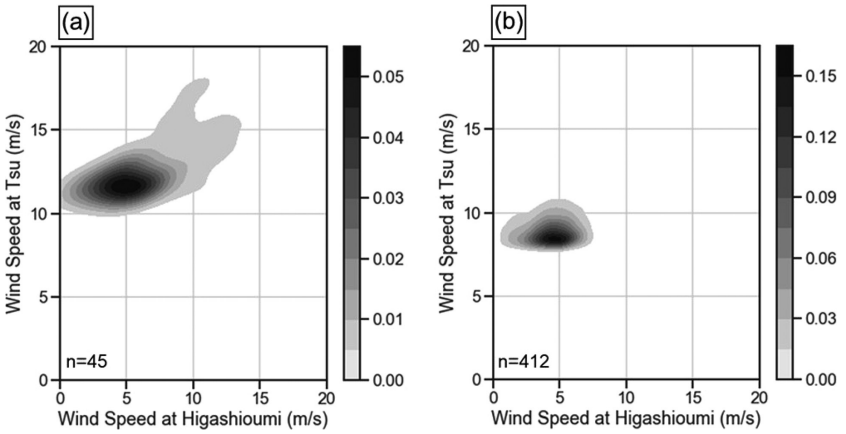

Fig. 6. Distribution of kernel density estimation of wind speeds simultaneously in Tsu and Higashiomi during the Suzuka-oroshi events. A darker color indicates a denser sample. (a) Suzuka-oroshi and (b) Weak-Suzuka-oroshi.

Table 4. Presence of inversion layer and wind speed approaching the mountains during Suzuka-oroshi events.

		Presence of the inversion layer		
		Presence	Absence	Missing data
Wind speed approaching the mountains ($m\ s^{-1}$)	0–6	13	0	0
	6–12	16	5	2
	> 12	2	4	0

the actual wind conditions, we investigated the vertical structure of Suzuka-oroshi using the simulation results. Figure 10 shows the temporal variation in the vertical cross-section of the potential temperature across the northern part of the mountains. At 1300 JST, a relatively strong stable layer flowed into the area at around 1.5–2 km altitude on the windward side (Fig. 10b). Simultaneously, a relatively weak wind region formed over the leeward slope of the Suzuka Mountains, and the isotherms decreased. From 1400 JST to 1500 JST, the amplitude of the mountain waves increased, creating flows that split the previously formed weak wind region up and down (Figs. 10c, d). The wind speed windward far from the mountains and on the leeward slopes gradually increased from 1500 JST to 1600 JST (Figs. 10d, e). On the basis of the vertical cross-section when the surface wind speed was the highest, the isentropes were largely drawn down along the leeward slope, and the wind speed in this direction increased by ~ 5 $m\ s^{-1}$ compared to that in the windward direction (Fig. 10e). At 1300–1600

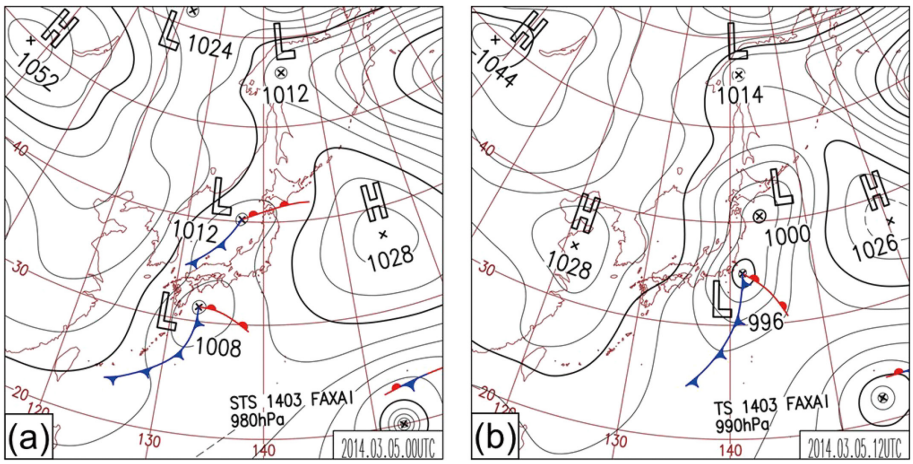

Fig. 7. Surface weather chart on March 5, 2014. (a) 0900 JST. (b) 2100 JST.

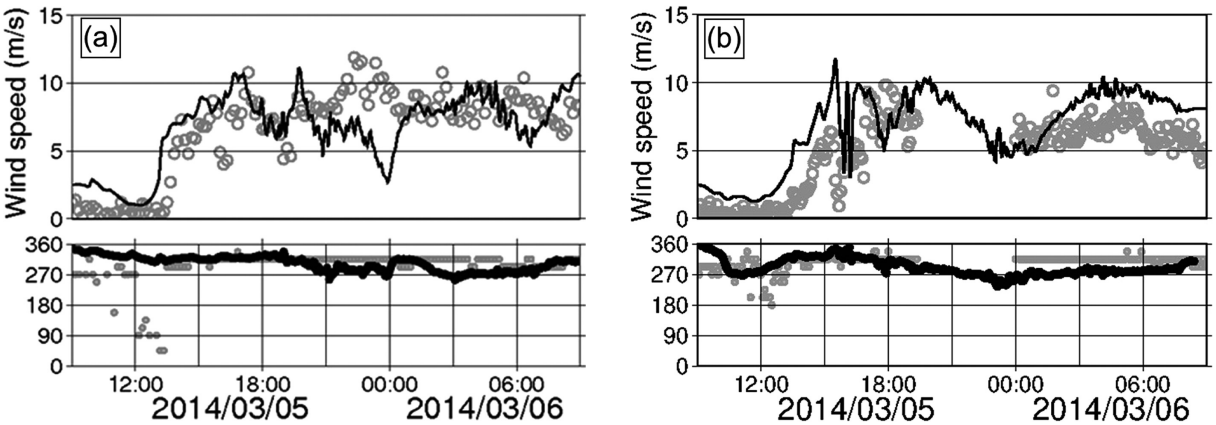

Fig. 8. Time series graphs of surface wind on March 5–6, 2014. (a) Tsu. (b) Komono.

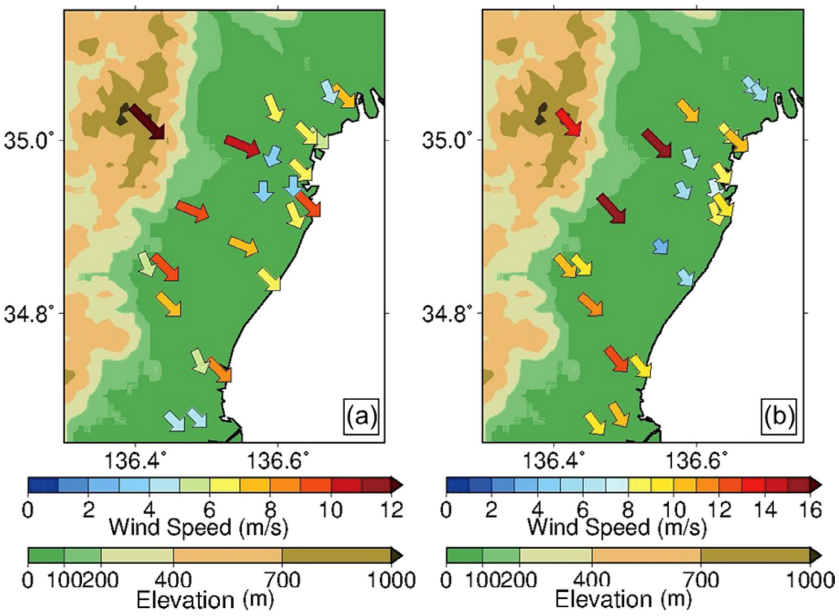

Fig. 9. Distribution of surface winds leeward of the Suzuka Mountains. (a) Results from observations at 1700 JST on March 5, 2014. (b) Results from CTRL simulation at 1700 JST on March 5, 2014.

JST, it seems that the flow undergoes a transition from subcritical on the windward side to supercritical flow on the lee slope. Indeed, internal Froude number ($Fi = U/\sqrt{g^* h}$) was lesser than 1.0 (approximately 0.5–0.8) at the windward and greater than 1.0 (approximately 1.6–2.9) above the leeward slope from 1300 JST to 1600 JST. Here, U and h are the wind speed and the depth of the duct (or inversion layer height), respectively. g^* is the reduced gravity constant, considering the potential temperature difference between the two layers ($g^* = \frac{\Delta\theta}{\theta} g$). In the leeward region of the mountains, the airflow jumps slightly on the ground level, and the ridge is located near the coast. A weak wind area near the ground level was generated in response to this ridge of mountain waves. Additionally, there was a relatively weaker wind region with large wave amplitude above the strong wind layer. These results reflect the general characteristics of downslope windstorms. Thereafter, as the inflow wind speed increased, the overall surface wind speed increased until 0000 JST on March 6, 2014, and then gradually decreased.

Conversely, the vertical cross-sections of the central and southern regions showed that the isentropes were not largely drawn down along the leeward slope of the mountains (Fig. 11). Therefore, the isotherms below 1 km altitude are not so dense over the leeward slope and plain. It is considered that the wind speed between the northern and southern parts differed because of differences in the height of the mountains.

Figure 12 shows the distribution of the deviations in the surface wind speed simulated from the CTRL case minus the results of the NoMt case. The presence of the Suzuka Mountains strengthened the surface wind speeds by approximately 4–6 m s^{-1} leeward of the mountains. Figures 10 and 12 show that Suzuka-oroshi was downslope winds caused by the topographic effect of the Suzuka Mountains.

4. Discussion

We found that Suzuka-oroshi blows not only in the southern part of the plain on the leeward side of the Suzuka Mountains but also in the northern and central parts. This finding agrees with anecdotal observations from local residents. The reasons for the difference in the strong wind areas found in this study compared to those of previous studies may be as follows: Owada (1990) did not survey the northern part of the plain leeward of the Suzuka Mountains. Additionally, Komatsu and Tachibana (2016) did not survey winds in the northern part of the plain near the mountain foothills. In the central part of the plain, they did not consider differences in the above-ground level of the AMeDAS anemometers at different observation stations. The AMeDAS anemometers installed in the central part are approximately 10 m lower than those installed in the southern part. This difference in height

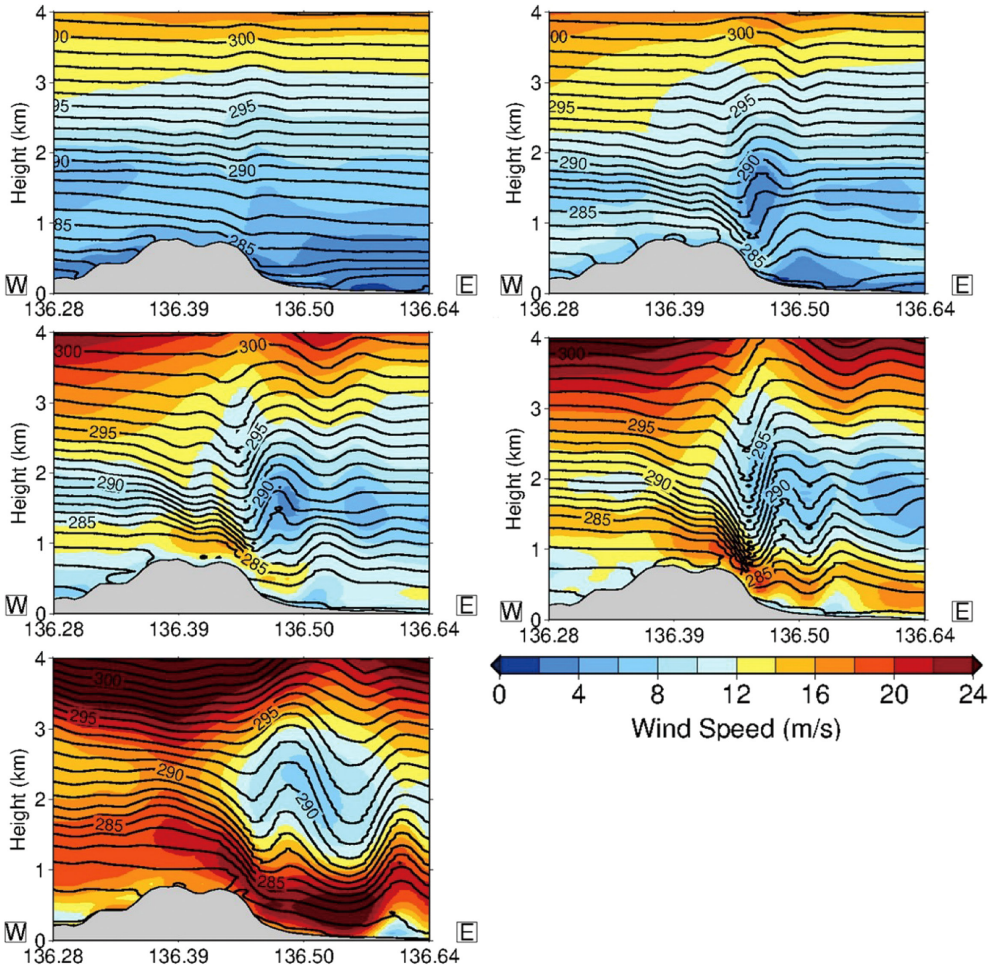

Fig. 10. Vertical cross-section of isentropes from CTRL simulation across the northern Suzuka Mountains (line A in Fig. 3) on March 5, 2014 (CTRL simulation). (a) 1200 JST. (b) 1300 JST. (c) 1400 JST. (d) 1500 JST. (e) 1600 JST.

leads to the underestimation of the wind speeds by 3 m s^{-1} in the central part of the plain, which may have prevented the detection of the strong winds in the central part of the plain by Komatsu and Tachibana (2016).

The results of the climatological analysis indicated that the atmospheric conditions were suitable for generating downslope winds in many Suzuka-oroshi events. When an inversion layer is present, downslope winds tend to occur, as described in Section 1. Note that the inversion layer is a supportive factor. If *Fr* is 0.6–1.2, the downslope windstorms tend to occur even when an inversion layer is absent (Lin and Wang 1996).

The results of the numerical simulation also revealed a slightly strong stable layer between the 1.5-km and 2.0-km levels in the windward and mountain ranges. Additionally, there were large-amplitude mountain waves and a weaker wind layer above the leeward slope of the Suzuka Mountains than in the surroundings; airflow below this weak wind region resulted in strong winds. Note that this weak wind region was not a typical mountain-wave breaking region above the mountain slope and did not develop a clear hydraulic jump. Such atmospheric conditions cannot form gusty, very strong downslope windstorms, such as the chinook and Yamaji-kaze, but can cause strong winds due to the transition of the flow regime, as shown by Durran (1990). Indeed, Suzuka-oroshi winds are stronger than the winds in windward areas but are not similar to chinook. The simulation results from the CTRL and NoMt cases supported the mountain effects on the strong winds and that Suzuka-oroshi exhibits

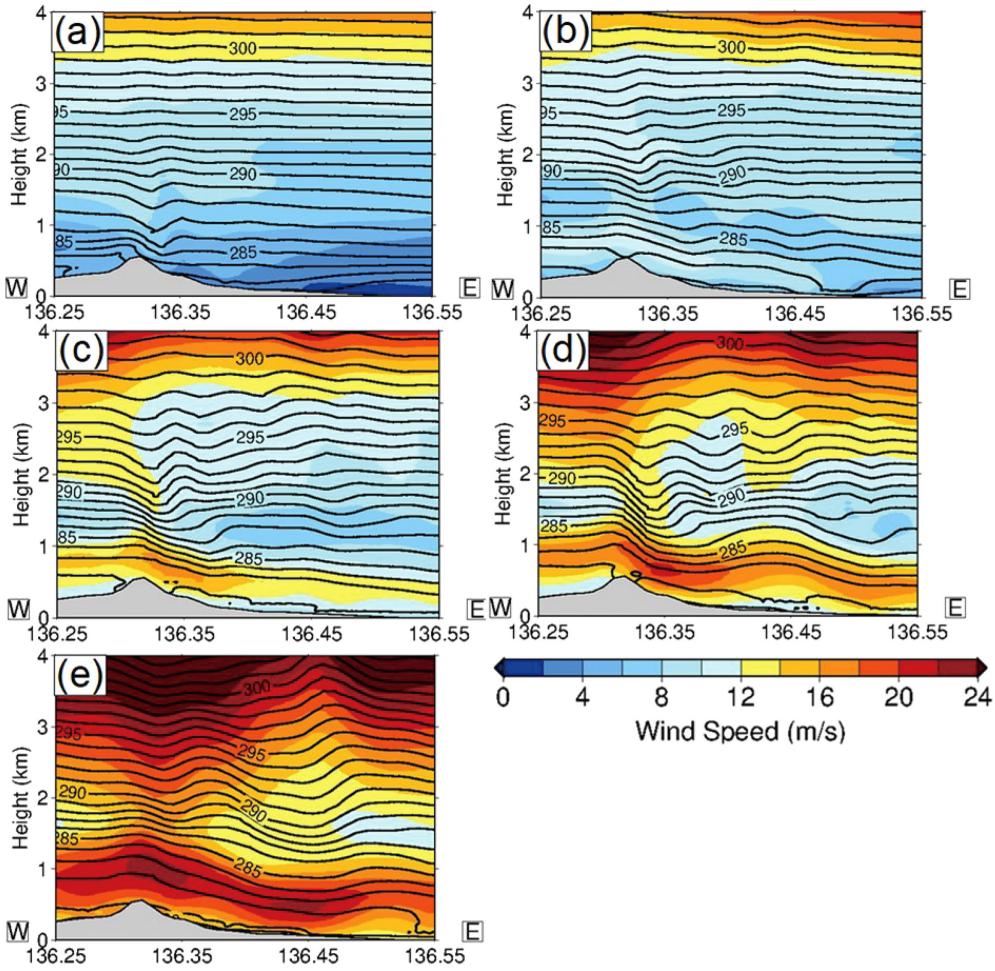

Fig. 11. Vertical cross-section of isentropes from CTRL simulation across the southern Suzuka Mountains (line B in Fig. 3) on March 5, 2014. (a) 1200 JST. (b) 1300 JST. (c) 1400 JST. (d) 1500 JST. (e) 1600 JST.

characteristics of downslope windstorms. The pre-existing or self-induced critical layer was not observed at the upper level (see figure in Appendix B). Thus, the Suzuka-oroshi in this case does not support the resonant amplification theory.

We simulated Suzuka-oroshi in only one case and discussed the mechanism. To improve the robustness of our results, additional cases should be evaluated. Particularly, the mechanism of Suzuka-oroshi with a clear inversion layer was not investigated in the simulations, but it will be examined in our further research.

5. Conclusions

Suzuka-oroshi blows in the southern parts of the plain on the leeward side of the Suzuka Mountains and in the northern part. The winds are strongest and more frequent near the foot of the mountain range in the northern part. These results differed from those of previous studies.

Suzuka-oroshi mainly occurs just after an extratropical cyclone with a cold front passing through the Sea of Japan (55 % of cases). Furthermore, an inversion layer at 1–5 km was found in 74 % of cases. Considering that Suzuka-oroshi tended to blow immediately after the passages of cold fronts, this inversion layer may be a frontal inversion layer. Suzuka-oroshi also blows at night.

Numerical simulations with the high-resolution WRF model supported this finding. Simulation results with and without the Suzuka Mountains demonstrated that the strong Suzuka-oroshi in the northern part of the plain comprised downslope windstorms with a

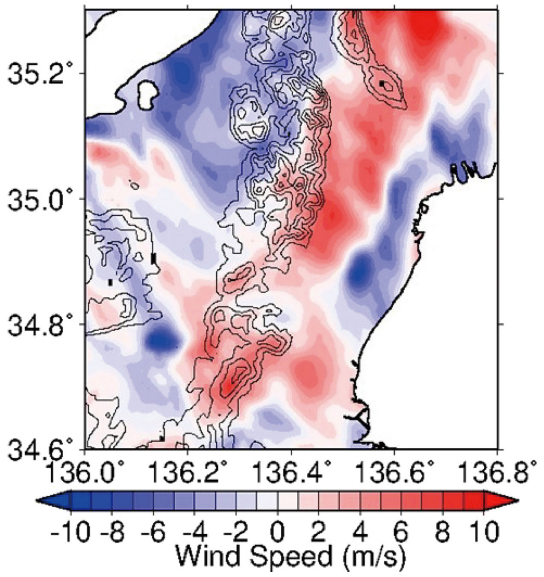

Fig. 12. Impacts of mountains on the surface wind speed (cases CTRL–NoMt) at 1700 JST on March 5, 2014.

transition of flow regime. Additionally, differences in the height of the mountains between the northern and southern parts resulted in the greater wind speed in the northern parts compared to the southern parts.

We determined the location, timing, and reasons for Suzuka-oroshi blowing. These results improve the understanding of local winds in Japan and may contribute to the safe operation and management of highways in this region.

Data Availability Statements

The datasets generated in this study will be available from the corresponding author upon reasonable request for the next five years.

Acknowledgments

This research was supported by the Environment Research and Technology Development Fund JPMEERF20192005 of the Environmental Restoration and Conservation Agency of Japan. This research was supported by the Multidisciplinary Cooperative Research Program of the Center for Computational Sciences, University of Tsukuba.

Appendix A

Distribution of surface winds leeward of the Suzuka Mountains. Results from observations on March 5, 2014, at (a) 1200 JST, (c) 1400 JST, and (e) 1600 JST.

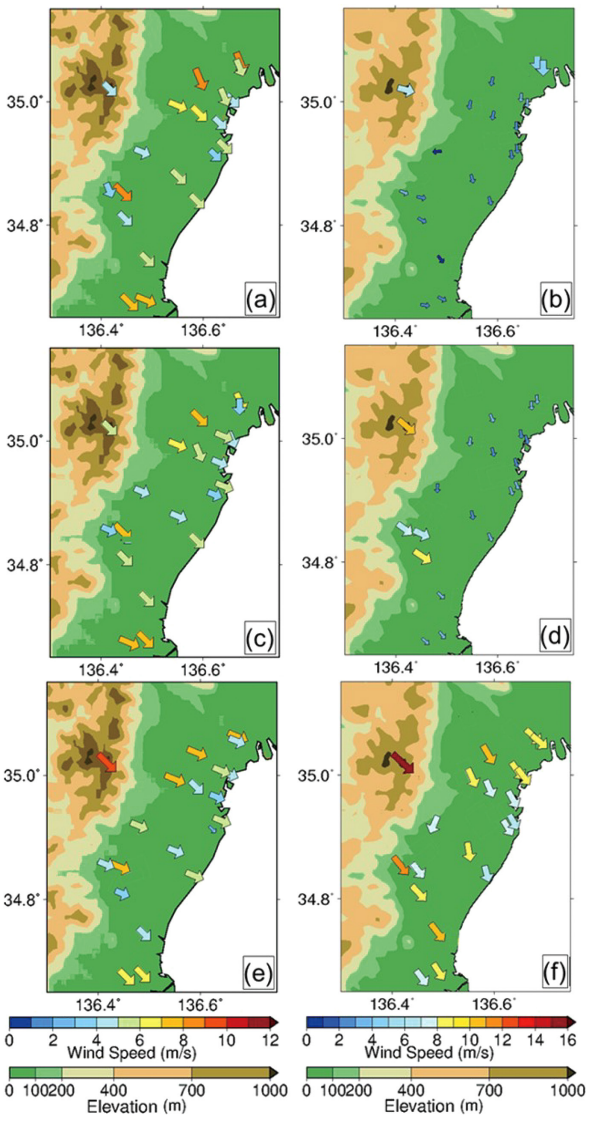

Fig. A1.

Results from CTRL simulation on March 5, 2014, at (b) 1200 JST, (d) 1400 JST, (f) and 1600 JST.

Appendix B

Vertical cross-section of wind speed to 10-km altitude from CTRL simulation across the northern Suzuka Mountains (line A in Fig. 3) at 1600 JST on March 5, 2014 (CTRL simulation). Shade and contour indicate horizontal wind speed (m s^{-1}) and potential temperature (K), respectively.

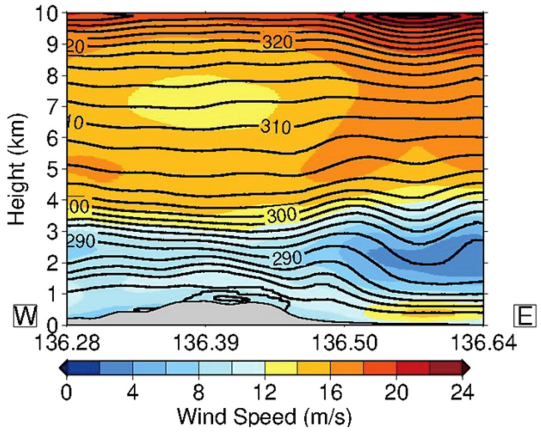

Fig. B1.

References

Arakawa, S., 1968: A proposed mechanism of fall winds and Dashikaze. *Pap. Meteor. Geophys.*, **19**, 69–99.

Arakawa, S., 1969: Climatological and dynamic studies on the local strong winds, mainly in Hokkaido, Japan. *Geophys. Mag.*, **34**, 359–425.

Armi, L., and G. J. Mayr, 2007: Continuously stratified flow across an Alpine crest with a pass: Shallow and deep föhn. *Quart. J. Roy. Meteor. Soc.*, **133**, 459–477.

Asano, Y., and H. Kusaka, 2022: Numerical simulation study of the effects of foehn winds on white head incidences in Yamagata Prefecture, Japan. *Meteor. Appl.*, **28**, e2042, doi:10.1002/met.2042.

Clark, T. L., and W. R. Peltier, 1984: Critical level reflection and the resonant growth of nonlinear mountain waves. *J. Atmos. Sci.*, **41**, 3122–3134.

Durran, D. R., 1986: Mountain waves. *Mesoscale Meteorology and Forecasting*. Ray, P. S. (ed.), Amer. Meteor. Soc. 472–492.

Durran, D. R., 1990: *Mountain Waves and Downslope Winds. Atmospheric Processes over Complex Terrain*. Meteor. Monogr., No. 23, Blumen, W. (ed.), Amer. Meteor. Soc., 59–81.

Durran, D. R., and J. B. Klemp, 1987: Another look at downslope winds. Part II: Nonlinear amplification beneath wave-overturning layers. *J. Atmos. Sci.*, **44**, 3402–3412.

Elvidge, A. D., and I. A. Renfrew, 2016: The causes of foehn warming in the lee of mountains. *Bull. Amer. Meteor. Soc.*, **97**, 455–466.

Elvidge, A. D., I. A. Renfrew, J. C. King, A. Orr, and T. A. Lachlan-Cope, 2016: Foehn warming distributions in nonlinear and linear flow regimes: A focus on the Antarctic Peninsula. *Quart. J. Roy. Meteor. Soc.*, **142**, 618–631.

Elvidge, A. D., P. K. Munneke, J. C. King, I. A. Renfrew, and E. Gilbert, 2020: Atmospheric drivers of melt on Larsen C ice shelf: surface energy budget regimes and the impact of foehn. *J. Geophys. Res.: Atmos.*, **125**, e2020JD032463, doi:10.1029/2020JD032463.

Fudeyasu, H., T. Kuwagata, Y. Ohashi, S. I. Suzuki, Y. Kiyohara, and Y. Hozumi, 2008: Numerical study of the local downslope wind "Hirodo-kaze" in Japan. *Mon. Wea. Rev.*, **136**, 27–40.

Gaberšek, S., and D. R. Durran, 2006: Gap flows through idealized topography. Part II: Effects of rotation and surface friction. *J. Atmos. Sci.*, **63**, 2720–2739.

Glennf, C. L., 1961: The Chinook. *Weatherwise*, **14**, 174–182.

Gohm, A., and G. J. Mayr, 2004: Hydraulic aspects of föhn winds in an Alpine valley. *Quart. J. Roy. Meteor. Soc.*, **130**, 449–480.

Gohm, A., and G. J. Mayr, 2005: Numerical and observational case-study of a deep Adriatic bora. *Quart. J. Roy. Meteor. Soc.*, **131**, 1363–1392.

Gohm, A., G. Mayr, A. Fix, and A. Giez, 2008: On the onset of bora and the formation of rotors and jumps near a mountain gap. *Quart. J. Roy. Meteor. Soc.*, **134**, 21–46.

Houghton, D. D., and A. Kasahara, 1968: Nonlinear shallow fluid flow over an isolated ridge. *Commun. Pure Appl. Math.*, **21**, 1–23.

Ishii, S., K. Sasaki, K. Mizutani, T. Aoki, T. Itabe, H. Kanno, D. Matsushima, W. Sha, A. T. Noda, M. Sawada, M. Ujiie, Y. Matsuura, and T. Iwasaki, 2007: Temporal evolution and spatial structure of the local easterly wind "Kiyokawa-dashi" in Japan. PART I: Coherent Doppler lidar observations. *J. Meteor. Soc. Japan*, **85**, 797–813.

Jackson, P. L., G. Mayr, and S. Vosper, 2013: Dynamically-driven winds. *Mountain Weather Research and Forecasting*. Chow, F. K., S. F. J. De Wekker, B. J. Snyder (eds.), Springer, 121–218.

Klemp, J. B., and D. R. Lilly, 1975: The dynamics of wave-induced downslope winds. *J. Atmos. Sci.*, **32**, 320–339.

Klemp, J. B., and D. R. Durran, 1987: Numerical modeling of Bora winds. *Meteor. Atmos. Phys.*, **36**, 215–227.

Komatsu, K. K., and Y. Tachibana, 2016: Two types of strong local wind captured by simultaneous multiple-site radiosonde soundings across a mountain range. *Mon. Wea. Rev.*, **144**, 3915–3936.

Koyanagi, T., and H. Kusaka, 2020: A climatological study of the strongest local winds of Japan "Inami-kaze". *Int. J. Climatol.*, **40**, 1007–1021.

Kusaka, H., and H. Fudeyasu, 2017: Review of downslope windstorms in Japan. *Wind and Structures*, **24**, 637–656.

Kusaka, H., Y. Miya, and R. Ikeda, 2011: Effects of solar radiation amount and synoptic-scale wind on the local wind "Karakkaze" over the Kanto Plain in Japan. *J. Meteor. Soc. Japan*, **89**, 327–340.

Kusaka, H., A. Nishi, A. Kakinuma, Q.-V. Doan, T. Onodera, and S. Endo, 2021: Japan's south foehn on the Toyama

Plain: Dynamical or thermodynamical mechanisms? *Int. J. Climatol.*, **41**, 5350–5367.

Nishi, A., and H. Kusaka, 2019a: A climatological study of the local "Karakkaze" wind, with a focus on temperature change. *SOLA*, **15**, 149–153.

Nishi, A., and H. Kusaka, 2019b: The "Karakkaze" Local wind as a convexity wind: A case study using dual-sonde observations and a numerical simulation. *SOLA*, **15**, 160–165.

Lilly, D. K., and E. J. Zipser, 1972: The front range windstorm of 11 January 1972 a meteorological narrative. *Weatherwise*, **25**, 56–63.

Lilly, D. K., and J. B. Klemp, 1979: The effects of terrain shape on nonlinear hydrostatic mountain waves. *J. Fluid Mech.*, **95**, 241–261.

Lin, Y.-L., 2007: *Mesoscale Dynamics*. Cambridge University Press, 630 pp.

Lin, Y.-L., and T.-A. Wang, 1996: Flow regimes and transient dynamics of two-dimensional stratified flow over an isolated mountain ridge. *J. Atmos. Sci.*, **53**, 139–158.

Miller, P. P., and D. R. Durran, 1991: On the sensitivity of downslope windstorms to the asymmetry of the mountain profile. *J. Atmos. Sci.*, **48**, 1457–1473.

Orr, A., G. J. Marshall, J. C. R. Hunt, J. Sommeria, C.-G. Wang, N. P. M. van Lipzig, D. Cresswell, and J. C. King, 2008: Characteristics of summer airflow over the Antarctic Peninsula in response to recent strengthening of westerly circumpolar winds. *J. Atmos. Sci.*, **65**, 1396–1413.

Owada, M., 1991: *A climatological study of local winds (Oroshi) in central Japan*. Doctoral Thesis, Inst. Geosci., Univ. Tsukuba, 88 pp. [Available at https://dl.ndl.go.jp/info:ndljp/pid/3072387?tocOpened=1.]

Peltier, W. R., and T. L. Clark, 1979: The evolution and stability of finite-amplitude mountain waves. Part II: Surface wave drag and severe downslope windstorms. *J. Atmos. Sci.*, **36**, 1498–1529.

Peltier, W. R., and T. L. Clark, 1983: Nonlinear mountain waves in two and three spatial dimensions. *Quart. J. Roy. Meteor. Soc.*, **109**, 527–548.

Pitts, R. O., and T. J. Lyons, 1989: Airflow over a two-dimensional escarpment. I: Observations. *Quart. J. Roy. Meteor. Soc.*, **115**, 965–981.

Raymond, D. J., 1972: Calculation of airflow over an arbitrary ridge including diabatic heating and cooling. *J. Atmos. Sci.*, **29**, 837–843.

Saito, K., 1993: A numerical study of the local downslope wind "Yamaji-kaze" in Japan. Part 2: Non-linear aspect of the 3-D flow over a mountain range with a col. *J. Meteor. Soc. Japan*, **71**, 247–272.

Saito, K., 1994: A numerical study of the local downslope wind "Yamaji-kaze" in Japan. Part 3: Numerical simulation of the 27 September 1991 windstorm with a non-hydrostatic multi-nested model. *J. Meteor. Soc. Japan*, **72**, 301–329.

Saito, K., and M. Ikawa, 1991: A numerical study of the local downslope wind "Yamaji-kaze" in Japan. *J. Meteor. Soc. Japan*, **69**, 31–56.

Sasaki, K., H. Kanno, D. Matsushima, W. Sha, T. Iwasaki, S. Ishii, K. Mizutani, M. Moriyama, K. Fukubori, M. Murai, and K. Yokoyama, 2005: An observational study of the local easterly strong wind "Kiyokawa-dashi" in the Shonai Plains, Yamagata. *J. Agric. Meteor.*, **60**, 725–728.

Sasaki, K., M. Sawada, S. Ishii, H. Kanno, K. Mizutani, T. Aoki, T. Itabe, D. Matsushima, W. Sha, A. T. Noda, M. Ujiie, Y. Matsuura, and T. Iwasaki, 2010: The temporal evolution and spatial structure of the local easterly wind "Kiyokawa-dashi" in Japan. PART II: Numerical simulations. *J. Meteor. Soc. Japan*, **88**, 161–181.

Sawada, M., T. Iwasaki, W. Sha, T. Yamazaki, H. Iwai, S. Ishii, K. Mizutani, T. Itabe, and I. Yamada, 2012: Transient downslope winds under the influence of stationary lee waves from the Zao mountain range. *J. Meteor. Soc. Japan*, **90**, 79–100.

Smith, R. B., 1985: On severe downslope winds. *J. Atmos. Sci.*, **42**, 2597–2603.

Smith, R. B., 1987: Aerial observations of the Yugoslavian bora. *J. Atmos. Sci.*, **44**, 269–297.

Smith, C. M., and E. D. Skyllingstad, 2011: Effects of inversion height and surface heat flux on downslope windstorms. *Mon. Wea. Rev.*, **139**, 3750–3764.

Turton, J. V., A. Kirchgaessner, A. N. Ross, and J. C. King, 2018: The spatial distribution and temporal variability of föhn winds over the Larsen C ice shelf, Antarctica. *Quart. J. Roy. Meteor. Soc.*, **144**, 1169–1178.

Wind Engineering Institute, Co., Ltd., 1984: *This Is All You Need to Know about Building Wind*. Kajima Institute Publishing, 224 pp (in Japanese).

Yoshino, M. M., 1975: *Climate in a Small Area: An Introduction to Local Meteorology*. University of Tokyo Press, 549 pp.

Yoshino, M. M., 1986: *Climate in a Small Area. New Edition.* Chijin Shokan, 298 pp (in Japanese).

Zängl, G., A. Gohm, and G. Geier, 2004: South foehn in the Wipp Valley–Innsbruck region: Numerical simulations on the 24 October 1999 case (MAP-IOP 10). *Meteor. Atmos. Phys.*, **86**, 213–243.